

pubs.acs.org/chemneuro Research Article

# Substoichiometric Inhibition of Insulin against IAPP Aggregation Is Attenuated by the Incompletely Processed N-Terminus of proIAPP

Nadav Benhamou Goldfajn, Huayuan Tang, \*, and Feng Ding\*



Cite This: ACS Chem. Neurosci. 2022, 13, 2006-2016



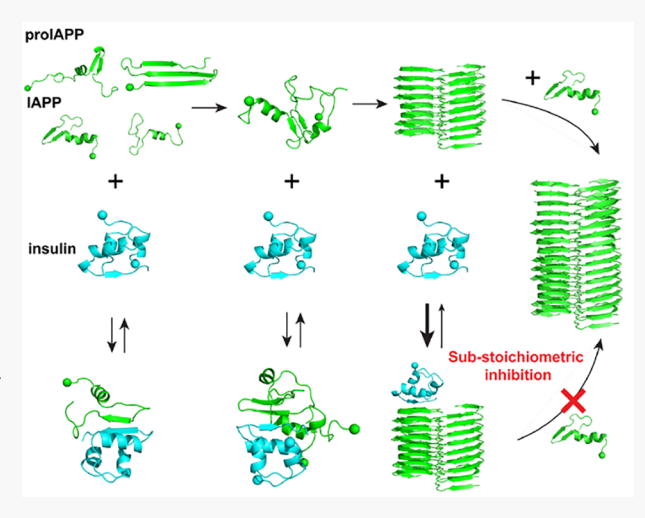
**ACCESS** 

Metrics & More

Article Recommendations

Supporting Information

ABSTRACT: Substoichiometric aggregation inhibition of human islet amyloid polypeptide (IAPP), the hallmark of type 2 diabetes impacting millions of people, is crucial for developing clinic therapies, yet it remains challenging given that many candidate inhibitors require high doses. Intriguingly, insulin, the key regulatory polypeptide on blood glucose levels that are cosynthesized, costored, and cosecreted with IAPP by pancreatic  $\beta$  cells, has been identified as a potent inhibitor that can suppress IAPP amyloid aggregation at substoichiometric concentrations. Here, we computationally investigated the molecular mechanisms of the substoichiometric inhibition of insulin against the aggregation of IAPP and the incompletely processed IAPP (proIAPP) using discrete molecular dynamics simulations. Our results suggest that the amyloid aggregations of both IAPP and proIAPP might be disrupted by insulin through its binding with the shared amyloidogenic core sequences. However, the N-terminus of proIAPP competed with the amyloidogenic core sequences for the insulin interactions, resulting in attenuated



inhibition by insulin. Moreover, insulin preferred to bind the elongation surfaces of IAPP seeds with fibril-like structure, with a stronger affinity than that of IAPP monomers. The capping of elongation surfaces by a small amount of insulin sterically prohibited the seed growth via monomer addition, achieving the substoichiometric inhibition. Together, our computational results provided molecular insights for the substoichiometric inhibition of insulin against IAPP aggregation, also the weakened effect on proIAPP. The uncovered substoichiometric inhibition by capping the elongation of amyloid seeds or fibrils may guide the rational designs of new potent inhibitors effective at low doses.

KEYWORDS: Type 2 diabetes, amyloid aggregation, substoichiometric inhibition, discrete molecular dynamics, amyloid seed

#### **■ INTRODUCTION**

Amyloid diseases, including Alzheimer's and Parkinson's disease and type 2 diabetes (T2D), are associated with aberrant self-assembly of normally soluble proteins into insoluble amyloid fibrils with toxic intermediates generated along the process.1 Amyloid aggregation of human islet amyloid polypeptide (IAPP) is found in the pancreas of most T2D patients and are related to the death of  $\beta$ -cells.<sup>2</sup> IAPP is hormone stored, produced, and secreted with insulin in the granules of pancreatic  $\beta$ -cells,<sup>3</sup> which is initially expressed as an 89-amino acid (aa) polypeptide in the endoplasmic reticulum.4 Mature IAPP is a 37-aa peptide produced by removing the N-terminal 22-aa signaling sequence in the endoplasmic reticulum, cleaving off the 19aa C-terminal sequence in the secretory granule to produce the proIAPP peptide with 48 aa and subsequently cutting off the first N-terminal 11 aa of the proIAPP (Figure 1A).4 In prediabetic patients, the enzyme processing proIAPP into IAPP is often overwhelmed with the overproduction of precursor proteins, which results in accumulation of incompletely processed proIAPP. proIAPP was found to contribute to the islet amyloid by forming intragranular amyloid, seeding the formation of mature IAPP amyloid and promoting interactions with proteoglycans of extracellular matrix.<sup>5–7</sup> However, most aggregation and mitigation studies to date have focused on IAPP; the exact role of proIAPP in T2D etiology is still unknown.

Numerous biomolecules have been explored to act as antagonists of IAPP amyloid aggregation and toxicity. The reported amyloid inhibitors included small molecules, 8-12 chaperone proteins, 13 antibodies, 14,15 nanoparticles, 16-20 and

Received: April 16, 2022 Accepted: June 2, 2022 Published: June 15, 2022





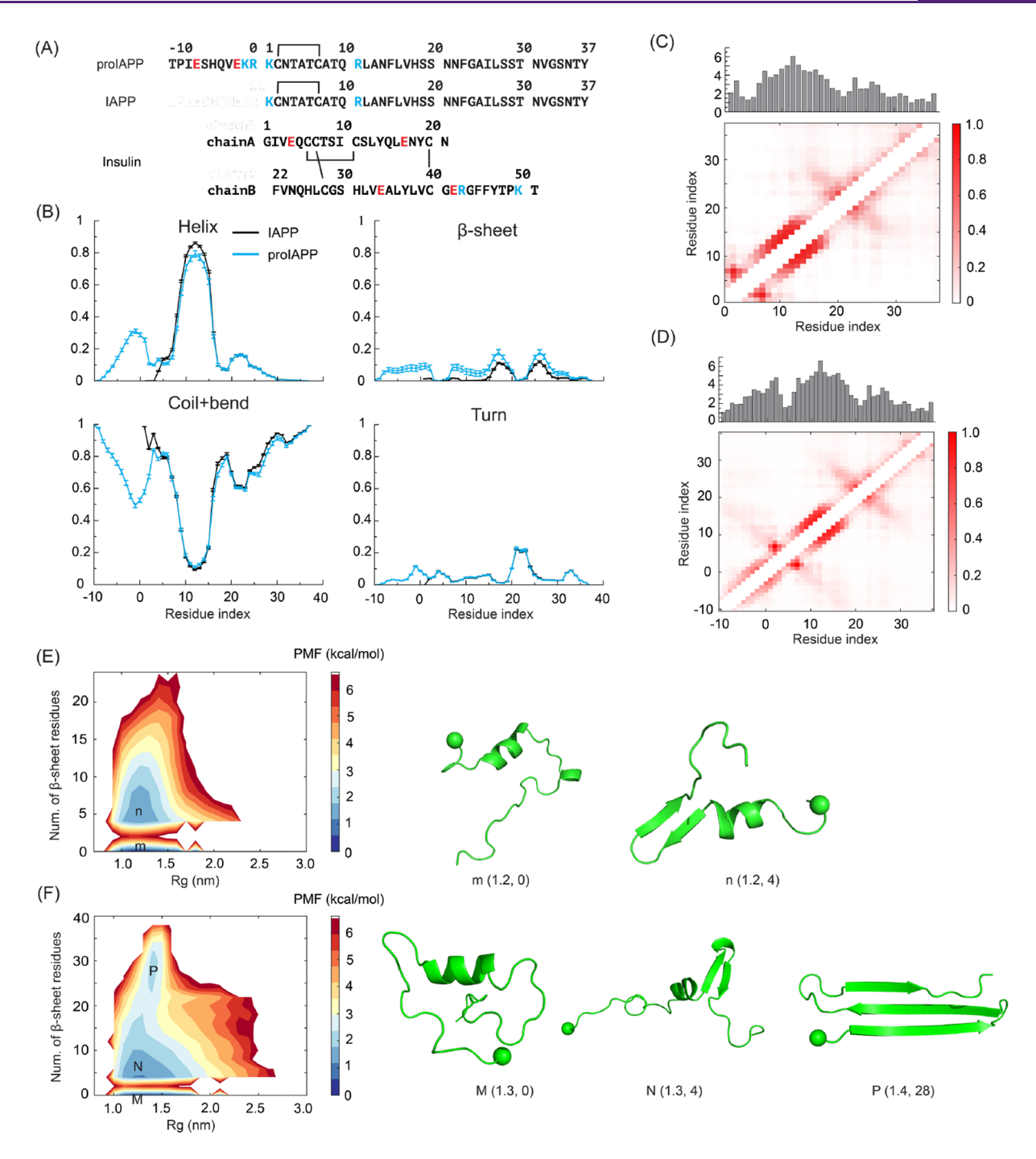


Figure 1. Structures of IAPP and proIAPP monomers. (A) Amino acid sequences of IAPP, proIAPP, and insulin with the positively and negatively charged residues highlighted in blue and red, respectively. Disulfide bonds are shown by black lines. (B) Secondary structure propensities of IAPP and proIAPP monomers. The results are presented as the mean  $\pm$  SEM of 50 independent simulations. (C, D) Residuewise intrapeptide contact frequency maps for (C) IAPP and (D) proIAPP. (E, F) Two-dimensional PMF with respect to the radius of gyration ( $R_g$ ) and number of  $\beta$ -sheet residues for (E) IAPP and (F) proIAPP monomers. The basins are labeled with the typical conformations presented on the right.

peptides. Among them, the peptide-based amyloid inhibitors are particularly attractive due to their high sequence specificity, selectivity, binding affinity, and biocompatibility, which can further be rationally designed and synthesized. Typical peptide-based amyloid inhibitors include  $\beta$ -strand mimics, helix mimetics, linear peptide derivatives, cyclic  $\beta$ -hairpin, and macrocycles. However, conventional inhibitors for IAPP amyloid aggregation usually require relatively high doses while design of substoichiometric inhibitors, crucial for clinic

application of high molecular weight peptide therapies, remains challenging. For instance, cyclic D,L- $\alpha$ -peptides required 10 times excess of concentrations to achieve a 55% reduction of amyloid  $\beta$  (A $\beta$ ) cytotoxicity. Macrocyclic peptides can effectively inhibit the amyloid aggregation of IAPP and A $\beta$  and reduce the cytotoxicities induced by cell membrane disruption at equimolar concentrations. Rat IAPP (rIAPP), which differs from human IAPP at six positions and does not form amyloid fibrils, 28,29 can only double the IAPP

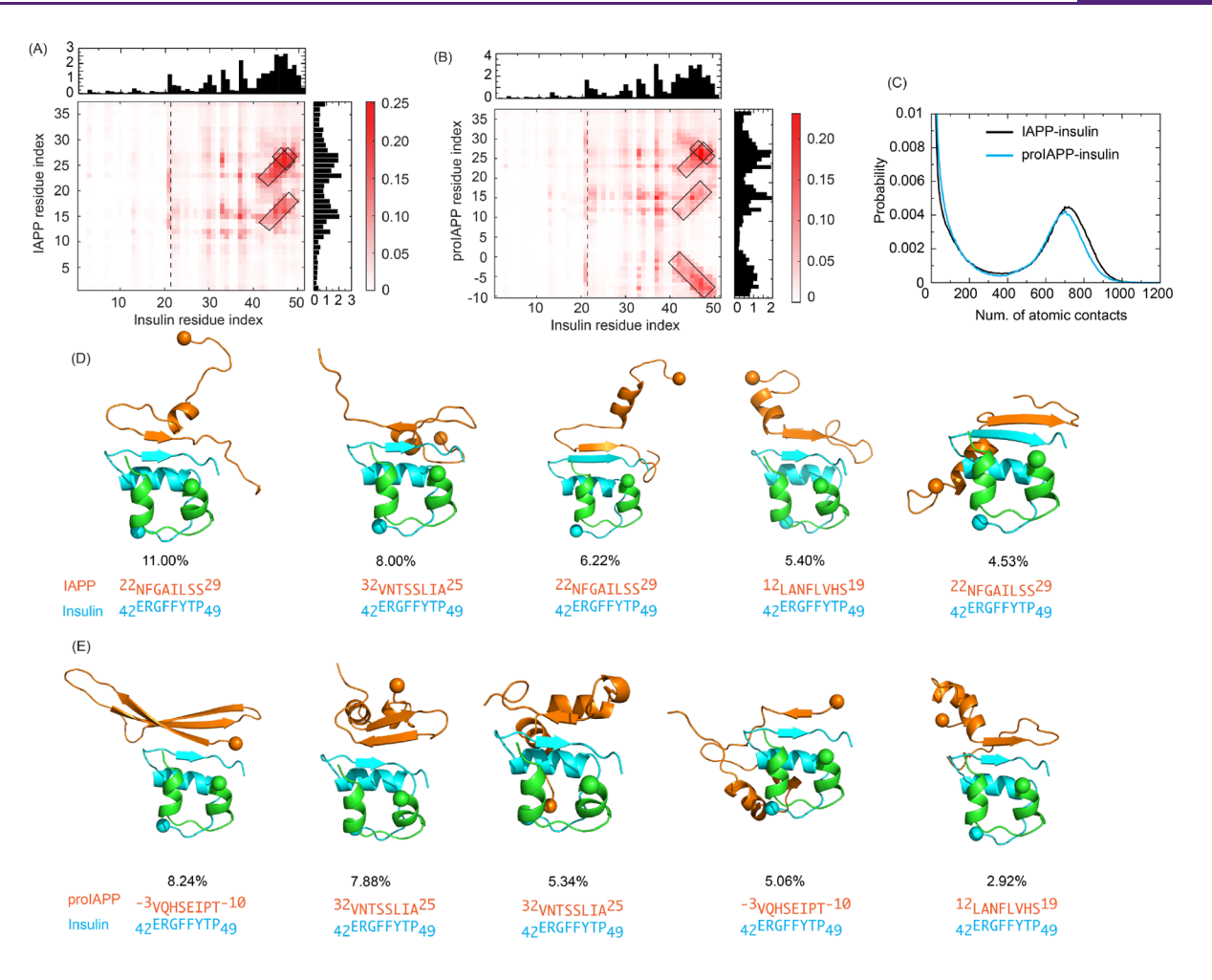


Figure 2. Binding of IAPP and proIAPP monomers with insulin. (A, B) Residuewise contact frequency maps between insulin and (A) IAPP, (B) proIAPP monomers. The hot spots of contacts are highlighted by boxes. The histograms of interpeptide contacts per residue were obtained by integrating the corresponding pairwise contact frequency map and are plotted on the top for insulin and right for IAPP or proIAPP residues, respectively. (C) Probability distribution of IAPP-insulin and proIAPP-insulin atomic contacts. (D, E) Top-five representative conformations of (D) IAPP-insulin and (E) proIAPP-insulin complexes obtained by clustering analysis with the proportion of the cluster and residues in contact indicated at the bottom of conformations.

aggregation time when the rIAPP/IAPP ratio is  $\sim$ 5. <sup>30</sup> Intriguingly, insulin, the key regulatory polypeptide for blood glucose levels that is co-produced, stored, and secreted with IAPP in the granules of pancreatic  $\beta$ -cells, has been identified as an exceptionally potent natural inhibitor of IAPP amyloid aggregation even at substoichiometric concentrations. For instance, the addition of 2  $\mu$ M insulin was found to increase the fibrillization time of 25  $\mu$ M IAPP by 8-fold. <sup>31</sup> Insulin was even capable of effectively inhibiting the aggregation of  $16~\mu$ M IAPP at a relatively low concentration of IAPP/insulin =  $100:1.^{32}$  A complete understanding of the molecular mechanism of insulin's substoichiometric inhibition against the amyloid aggregations of IAPP and proIAPP may provide important guidelines for the rational design of new peptide-based inhibitors.

Extensive investigations have been conducted to probe the interactions between insulin and IAPP peptides. Insulin is a globular protein consisting of two chains A and B, which are cross-linked by two disulfide bonds (Figure 1A). By dividing insulin into consecutive overlapping peptide arrays and investigating its binding with IAPP peptides separately, the residues 8–25 and 20–30 of insulin chain B were identified as

the binding sites for IAPP.<sup>33</sup> By use of a reciprocal peptide array, residues 7–19 of IAPP were recognized to bind insulin.<sup>33</sup> The  $\pi$ – $\pi$  stacking interaction between Y16 in insulin and F19 in IAPP was identified to play a crucial role in stabilizing the complexes formed by insulin and IAPP fibrils.<sup>34</sup> The inhibition effects of insulin depended on the insulin oligomeric state, as the binding regions of insulin for IAPP coincided with the insulin–insulin binding interface.<sup>35</sup> Compared to IAPP, proIAPP was found to be less amyloidogenic *in vitro*, but the inhibition effect of insulin is less effective against proIAPP than IAPP.<sup>32,36</sup> Despite these advances, the molecular mechanisms of the substoichiometric inhibition of insulin against the aggregation of IAPP as well as the incompletely processed proIAPP remain to be resolved.

In this study, we investigated the molecular mechanisms of substoichiometric inhibition of IAPP and proIAPP amyloid aggregation by insulin using discrete molecular dynamics simulations (DMD, see Methods), a predictive and efficient molecular dynamics engine with enhanced sampling efficiency. The interactions of insulin with IAPP and proIAPP in monomeric, oligomeric, and fibrillar states were probed by long time simulations ( $\sim$ 50  $\mu$ s accumulative simulation time

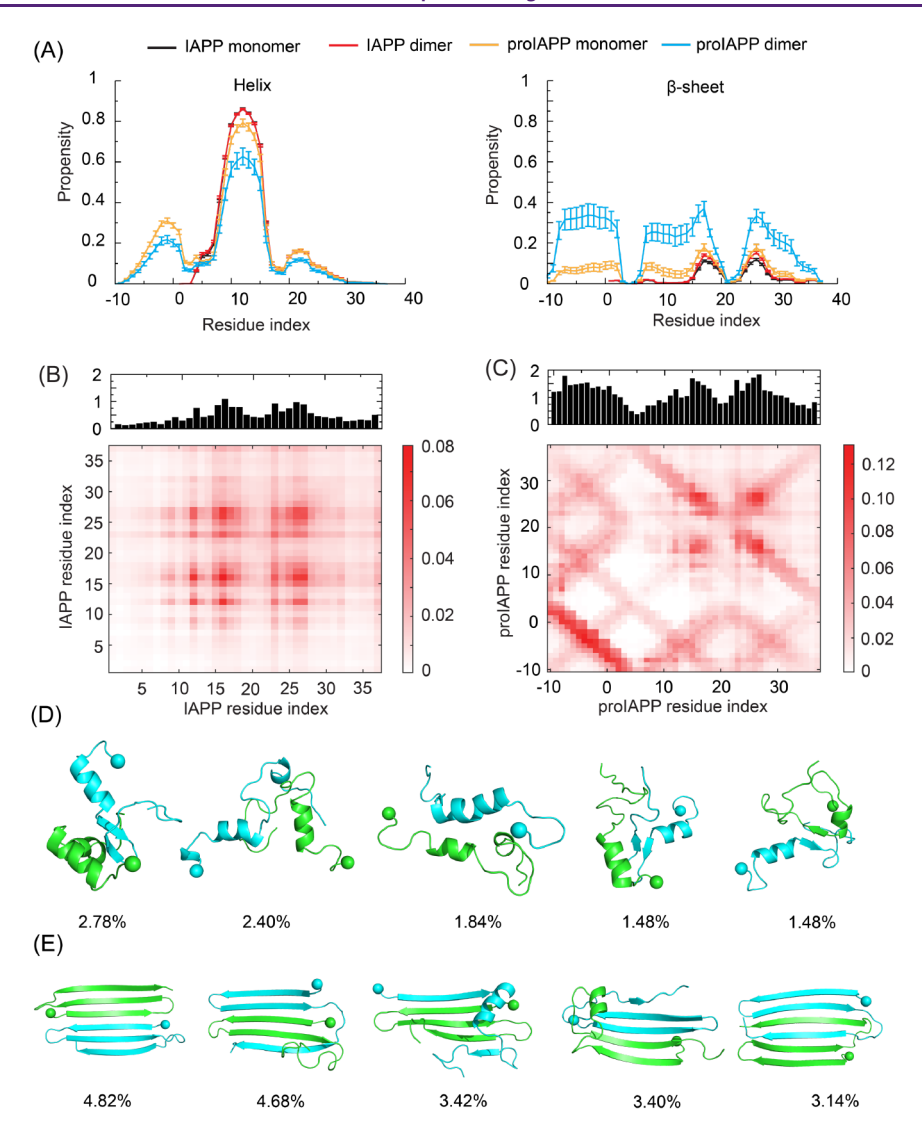


Figure 3. Dimerizations of IAPP and proIAPP. (A) Helical and β-sheet propensities of each residue in IAPP and proIAPP dimers. The results are presented as the mean ± SEM of 50 independent simulations. (B, C) Residuewise interpeptide contact frequency maps for (B) IAPP and (C) proIAPP dimers. (D, E) Top-five representative conformations obtained by clustering analysis for (D) IAPP and (E) proIAPP dimers with the N-terminal residues indicated by spheres.

for each molecular system). We found that insulin tended to bind and form intermolecular  $\beta$ -sheets with the amyloidogenic regions of IAPP and disrupt the interpeptide interactions in the self-assembly of IAPPs. The N-terminus of proIAPP competed with the amyloidogenic region near the C-terminal for the insulin interaction, thus weakening the inhibition effects of insulin in consistency with experimental results.<sup>32</sup> Moreover, insulins can tightly bind to the elongation surfaces of IAPP fibrils with preformed  $\beta$ -sheets, resulting in a stronger binding affinity than that with the intrinsically disordered IAPP monomers. The binding of insulin capped the IAPP fibril elongation surface by sterically prohibiting the fibril growth via monomer addition. By capping the growth of emerging fibril seeds during the lag-phase, a small amount of insulin can thus achieve substoichiometric inhibition of IAPP amyloid aggregation against the onset of T2D.

#### ■ RESULTS AND DISCUSSION

Both IAPP and proIAPP Monomers Were Intrinsically Disordered with Short Helices. The structures of IAPP and

proIAPP monomers were investigated by 50 independent DMD simulations with random initial velocities to ensure sufficient sampling, accumulating about 50  $\mu$ s of simulation time in total. Both IAPP and proIAPP were intrinsically disordered with the coil and bend being the predominant secondary structures (Figure 1B). The sequence index of proIAPP started from −10 such that the common sequence with IAPP had the same index. Residues 1-37 of proIAPP and IAPP shared similar ordered secondary structures, with residues 8-15 of high propensities to form helical structures and residues 16-20 and 24-28 of weak propensities to adopt  $\beta$ -sheet structures. Residuewise contact frequency map revealed interaction patterns of residues 8-15 along the diagonal and between residues 16-20 and 24-28 perpendicular to the diagonal (Figure 1C), consistent with corresponding secondary structures. The first 11 residues of proIAPP tended to form a helical structure with a lower propensity than the helix of residues A8-F15. Meanwhile, the N-terminus of the proIAPP can form  $\beta$ -hairpin with residues 10-20, as indicated by the contact pattern perpendicular to the diagonal

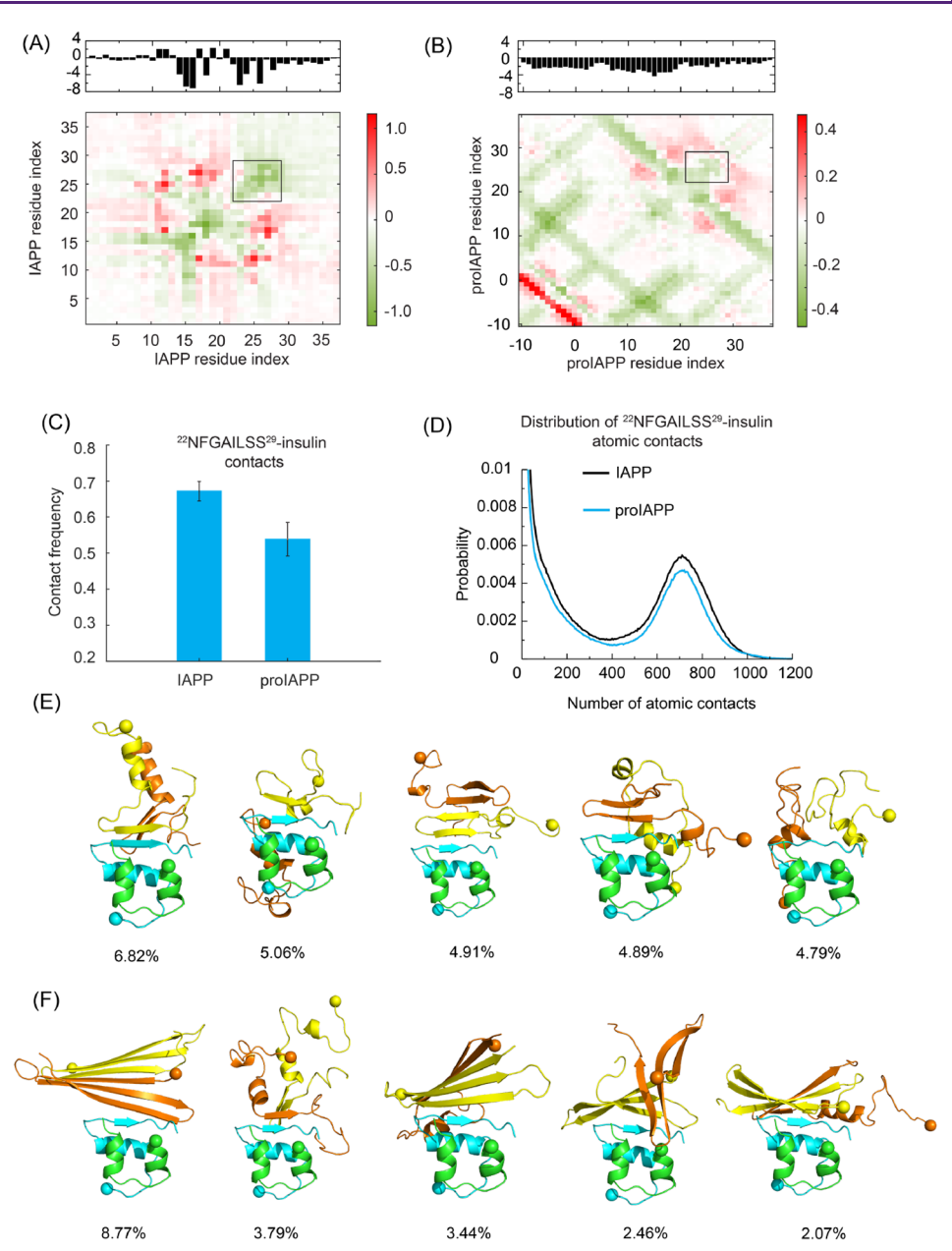


**Figure 4.** Inhibition of the dimerizations of IAPP and proIAPP by insulin. (A, B) Residuewise interpeptide contact frequency changes  $\Delta c = (C - C_0)/\text{max}(C_0)$  for (A) IAPP and (B) proIAPP dimers induced by the presence of insulin, where C and  $C_0$  are the respective contact frequencies in the presence and absence of insulin. (C) Contact frequencies between the amyloidogenic region <sup>22</sup>NFGAILSS<sup>29</sup> and insulin. (D) Histogram of the atomic contacts between <sup>22</sup>NFGAILSS<sup>29</sup> and insulin. (E, F) Top-five representative conformations obtained by clustering analysis for (E) IAPP and (F) proIAPP dimers.

in the contact frequency map (Figure 1D). To better understand of the structures of IAPP and proIAPP, we calculated the two-dimensional potential of mean force (PMF) with respect to the radius of gyration ( $R_{\rm g}$ ) and number of  $\beta$ -sheet residues (Figure 1E,F). The  $\beta$ -sheet residue number and  $R_{\rm g}$  of IAPP and proIAPP were sampled in a broad range of distributions, indicating the disordered feature of the peptides. The free-energy landscape of IAPP had two basins, with basin m featuring totally unstructured conformation and base n representing conformations with low  $\beta$ -sheet structures formed between residues 16–20 and 24–28 (Figure 1E). In contrast, there was a third basin P on the free-energy landscape of proIAPP, characterized by a high  $\beta$ -sheet structure content where the first 11 residues in the N-terminus -10-0, residues

16–20, and 24–28 in the C-terminus formed a three-strand  $\beta$ -sheet (Figure 1F). Taken together, IAPP and proIAPP monomers were highly disordered, and the N-terminus of proIAPP had weak tendencies to form ordered structures of both helix and  $\beta$ -sheet via intrapeptide interactions.

Insulins Bound with the Amyloidogenic Region of IAPP, while the Incompletely Processed N-Terminus of proIAPP Competed for Insulin Binding. To reveal the interaction mechanisms of insulin with IAPP and proIAPP, we first simulated either an IAPP or a proIAPP monomer with an insulin. The residuewise interpeptide contact frequencies between IAPP or proIAPP and insulin were calculated and averaged by all the independent simulations after reaching steady states (Figure 2A). The intermolecular interactions

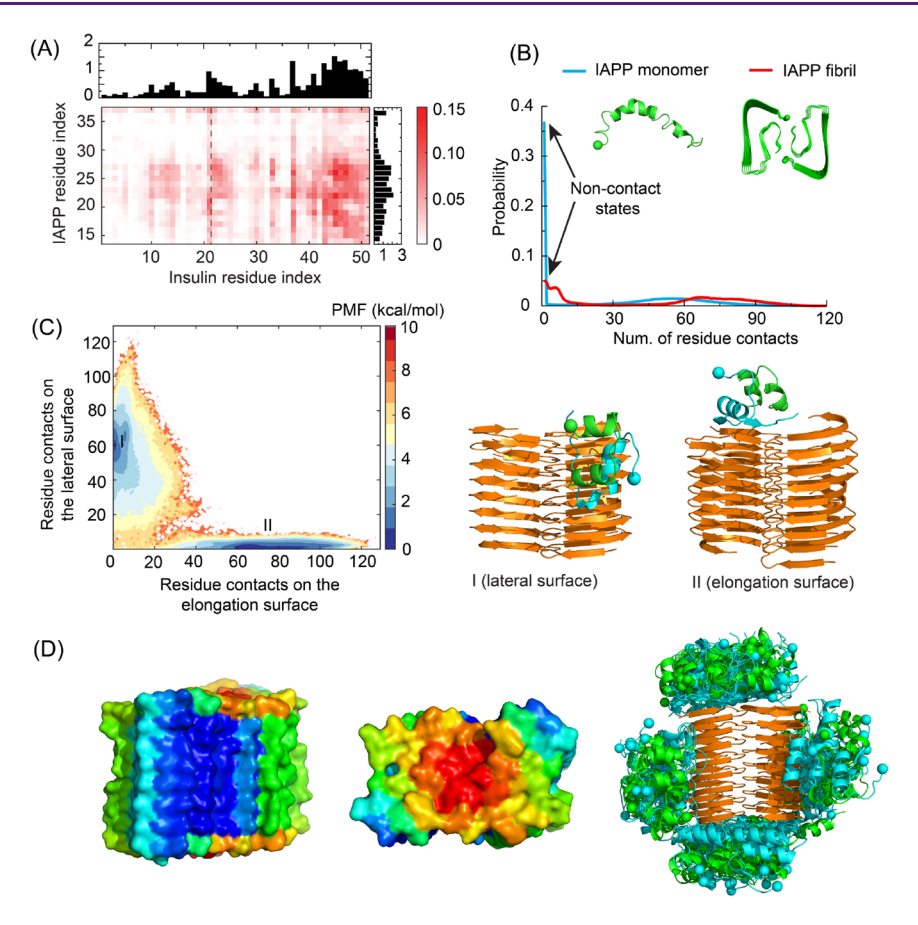


Figure 5. Insulin capped on lateral and elongation surfaces of an IAPP fibril. (A) Residuewise contact frequency map for insulin with elongation surface of an IAPP fibril. (B) Histogram of residue contacts between insulin and IAPP monomer and fibril. (C) Two-dimensional PMF with respect to the residue contacts on the lateral surface and elongation surface. The two basins are labeled with representative conformations shown at right. (D) Binding frequency of insulin with IAPP fibril. The IAPP fibril is represented by its surface with the molecular surface colored according to each residue's binding frequency from low (blue) to high (red). Left panel: front viewpoint. Middle panel: top viewpoint. Right panel: overlaying of final snapshots from 50 independent simulations.

between IAPP and insulin were predominantly contributed by residues 22–29 and 13–19 of IAPP, the primary and secondary amyloidogenic core regions of IAPP,  $^{39,40}$  and the residues 42–49 in the C-terminus of insulin chain B, consistent with previous work. The interactions can be found between chain A of insulin with IAPP. The interactions with insulin enhanced the formation of  $\beta$ -sheet structures between residues 22–29 and 13–19 of IAPP (Figure S1). Representative conformations obtained by clustering analysis showed that residues 22–29 and 13–19 of IAPP formed parallel and antiparallel  $\beta$ -sheet structures with the residues 42–49 of insulin (Figure 2D).

For the proIAPP monomer, most of its interaction with insulin occurred with the C-terminus of insulin chain B, similar to that with IAPP. Intriguingly, the N-terminus of proIAPP tended to form antiparallel  $\beta$ -sheet structures with the C-terminus of insulin chain B, in addition to the residues 22–29 and 13–19 of proIAPP (Figure 2B). The interactions with insulin significantly enhanced the  $\beta$ -sheet propensities in these regions (Figure S2). Importantly, the N-terminus of proIAPP competed with the amyloidogenic regions for the overlapped binding site in the insulin. Thus, the contacts between insulin and the proIAPP amyloidogenic regions, which were necessary for insulin to inhibit the amyloid aggregation of proIAPP, were mitigated (Figure 2C), as revealed by the histogram of atomic

contacts of IAPP and proIAPP with insulin. As indicated by the representative conformations obtained with the clustering analysis, the largest conformation cluster of proIAPP-insulin complexes involved antiparallel  $\beta$ -sheet structures formed by the N-terminus of proIAPP and the C-terminus of insulin (Figure 2E). Thus, the inhibition effect of insulin on the amyloid aggregation of proIAPP was weaker than that on the IAPP, supporting the experimental observation.<sup>32</sup>

Insulin Disrupted IAPP and proIAPP Dimerization by Hindering Self-Association Interactions between Amyloidogenic Regions. We next investigated the effects of insulin on the self-assembly of IAPP or proIAPP by simulating the dimerization of IAPP and proIAPP with and without the presence of an insulin. For each molecular system, 50 independent simulations were performed starting with randomized molecular positions and orientation and a minimum intermolecular atomic distance of 1.5 nm. Compared to IAPP monomer, the dimerization of IAPP alone was characterized by the increase of  $\beta$ -sheet structure between residues 16-20 and 24-28, while the helical propensities of each residue remained almost unchanged (Figure 3A, Figure S3). Relatively high interpeptide contact frequencies were identified between residues 16-20 and 24-28 (Figure 3B). The overall interpeptide contact frequency was low, suggesting the dimerization of IAPP peptide was a dynamic process

involving frequent association and dissociation. The IAPP dimers were stabilized by weak interactions with most residues adopting disordered structures (Figure 3D). In contrast, significant conformational conversions were observed during the dimerization of proIAPP. Upon dimerization, the helical structures at residues -10-0, 6-15, and 21-26 were converted to  $\beta$ -sheet structures with the  $\beta$ -sheet propensities reaching  $\sim 0.30$  (Figure 3A). The overall interpeptide contact frequency of proIAPP was higher than IAPP (Figure 3C). Various diagonal and antidiagonal contact patterns can be identified in the interpeptide contact frequency map, suggesting the proIAPP dimers were rich with parallel and antiparallel  $\beta$ -sheet structures (Figure 3E). The presence of intermediate states with the prevalence of out-register  $\beta$ -sheet would prohibit the nucleation of proIAPP fibrils that consist of in-register parallel  $\beta$ -sheet structures, in agreement with ThT experiments that the aggregation lag time of proIAPP was longer than that of IAPP<sup>32</sup> and electron microscopic experiments that ProIAPP had a strong potential to aggregate into ordered but nonfibrillar structures.3

In the presence of insulin, the diagonal region of interpeptide contact frequency between IAPP residues 15-21 and 22-29 was reduced, whereas off-diagonal contacts between residues 15-21 and 22-29 increased, suggesting that insulin prohibited the formation of in-register  $\beta$ -sheet structures and facilitated out-of-register  $\beta$ -sheet structures (Figure 4A). For proIAPP dimers, both in-register and out-ofregister  $\beta$ -sheet structures were reduced in the presence of insulin except the first 11 residues in the N-terminus, where the formation of antiparallel  $\beta$ -sheet structures was significantly enhanced (Figure 4B). Moreover, the reduction of interpeptide contacts between the primary amyloidogenic core of residues 22-29 of proIAPP was weaker compared with IAPP dimers (boxed regions in Figure 4A,B), consistent with experimental observations that the inhibition effect of insulin was weaker on proIAPP than IAPP aggregation.<sup>32</sup> The overall contact frequency between insulin and the primary amyloidogenic core of proIAPP was lower than that with IAPP (Figure 4C), confirming that insulin was less effective in prohibiting the assembly of the proIAPP amyloidogenic regions. The histograms of atomic contacts indicated that the IAPP-insulin and proIAPP-insulin contact states can be divided into a lowcontact state and a high-contact state (Figure 4D). Both the probabilities of low- and high-contact states of proIAPP were lower compared with IAPP. The representative conformations obtained by clustering analysis showed that the IAPP dimers bound with the insulin was highly disordered with one of the amyloidogenic regions interacting with the insulin (Figure 4E), whereas the proIAPP dimers were rich with intrapeptide  $\beta$ sheet structures that protected the amyloidogenic region from binding with the insulin (Figure 4F). Thus, the reduced inhibition effect of insulin on proIAPP aggregation may be attributed to the multiple intrapeptides  $\beta$ -sheet structures that prevented the proIAPP amyloidogenic region from interacting with insulin.

Insulins Substoichiometrically Inhibited IAPP Aggregation by Binding and Sterically Capping the Elongation Surfaces of IAPP Fibrils. The above discussions demonstrated that the aggregation of IAPP could be inhibited with an equimolar amount or 0.5 equiv of insulin. However, insulins were reported to inhibit the aggregation of IAPP peptides at substoichiometric concentration effectively, e.g., even at a very low molar ratio of IAPP/insulin = 100:1.<sup>32</sup> Thus,

the molecular mechanism of the substoichiometric inhibition of insulin on IAPP aggregation remains unclear. Here we investigated the interaction of insulin with a preformed IAPP fibril comprised of 16 peptides, recently solved by cryo-EM.  $^{41-43}$  The fibril with in-register  $\beta$ -sheet structures modeled the amyloid seed generated in the lag phase. The fibril was kept static to reduce computational cost, while the insulin was allowed to move freely (Methods). After the systems reached steady states, the residues 15-29 of IAPP fibril were found to display a high contact frequency with the residues 41-50 of insulin chain B (Figure 5A), similar to the binding pattern of insulin with a monomeric IAPP. Residue Y37 of insulin chain B was also identified to have a high binding affinity for IAPP fibrils, consistent with previous results that Y37 of insulin played an important role in stabilizing the insulin-IAPP fibril complex.<sup>34</sup> To compare the binding behaviors of insulin with IAPP monomers and fibrils, we calculated the distribution of residue contacts in each case (Figure 5B). The results showed that IAPP fibrils had a higher probability to make contact with insulin than IAPP monomers, and the number of residue contacts with peak probability was also larger for IAPP fibrils than monomers, suggesting IAPP fibrils entailed a strong binding with insulin than the IAPP monomers. To obtain more detailed information, we monitored the contacts between insulin and IAPP fibrils (e.g., 10 randomly selected simulation trajectories in Figure S4). IAPP monomers constantly associated and disassociated with insulin (Figure S4A), whereas the complexes formed by insulin and IAPP fibril were quite stable with rare disassociation observed (Figure S4B). Thus, the IAPP fibril had a stronger bind affinity with insulin than the IAPP monomer, which can be attributed to the aligned  $\beta$ -sheet structures of IAPP fibrils that facilitated the formation of interpeptide hydrogen bonds, whereas the conversion of IAPP monomers from disordered to ordered structures required extra entropy loss.

To describe the binding of insulin on the IAPP fibril, twodimensional PMF with respect to the residue contacts on the elongation surface and lateral surface of IAPP fibril was calculated (Figure 5C). The PMF featured two local basins I and II, corresponding to insulin binding on the lateral and elongation surfaces, respectively. The free energy of basin II was lower than basin I, suggesting that insulin preferred to bind the elongation surface of IAPP fibrils. As indicated by the time evolution of residue contacts on the lateral and elongation surfaces of typical trajectories, insulins that initially bound the lateral IAPP fibril surface could diffuse and convert to bind on the elongation surface in some cases (Figure S5). The binding frequency between insulin and each IAPP residue after reaching steady states was shown in Figure 5D. The amyloidogenic core residues on the elongation IAPP fibril surface displayed higher binding probabilities with insulin, while the binding with the lateral surface was weaker, especially given the fact that residues 19–30 were buried inside the fibril. As indicated by the conformations of insulin-IAPP fibril complexes (Figure 5C,D), the exposed helical structures of insulin bound on the elongation surface of IAPP fibril were not compatible with the fibril structures. Thus, the high binding affinities between the amyloidogenic cores of IAPP elongation surfaces and insulin enabled capping of insulins to sterically prevent the fibrillar growth of IAPP, which led to the substoichiometric inhibition of insulin on IAPP aggregation. During the lag phase of IAPP amyloid aggregation, the emerging IAPP fibril seeds are expected to have similar inregister  $\beta$ -sheets as mature IAPP fibrils. The high binding affinity of insulin with these IAPP seeds and subsequent inhibition of their growth would provide a robust inhibition of IAPP aggregation than the mechanism based on interactions with monomeric IAPP peptides. Although we focused on IAPP fibrils due to the lack of solved proIAPP fibril structures, the obtained interaction modes are expected to be valid also for proIAPP fibrils as the N-terminus of IAPP was disordered in fibrils without clear density, 41-43 which on the other hand would be available to compete with the IAPP amyloidogenic region in the elongation surface for binding with insulin.

In summary, we investigated the molecular mechanisms for the substoichiometric inhibition of peptide-based inhibitors against amyloid aggregation by studying the interactions of insulin with IAPP and proIAPP monomers, dimers, and fibrils. We found that the C-terminus of insulin chain B could bind both the primary and secondary amyloidogenic cores of IAPP by forming parallel or antiparallel intermolecular  $\beta$ -sheets. Thus, the insulin binding was found to disrupt the selfassembly of the amyloidogenic cores during the dimerization of IAPP because of the overlap between IAPP-IAPP and IAPP-insulin binding regions. The unprocessed N-terminal residues of proIAPP also exhibited a high binding propensity with the same C-terminus of insulin chain B, competing with the amyloidogenic regions for insulin binding. As a result, the inhibition effect of insulin on proIAPP dimerization was weaker than IAPP, consistent with experimental results.<sup>32</sup> Our results indicated that despite the high sequence similarity with IAPP, proIAPP exhibited a distinct aggregation behavior as well as a different interaction pattern with insulin due to the extra N-terminus of proIAPP.

Our simulations demonstrated that the interactions of insulin with IAPP and proIAPP monomers and dimers were highly dynamic involving frequent association and dissociation. Hence, the binding of insulin with IAPP monomers and dimers could not explain the substoichiometric inhibition of IAPP aggregation. In contrast, the binding of insulin on the elongation surface of IAPP fibrils was more energetically favored with a low dissociation rate because of the prealigned in-register  $\beta$ -sheet structures in the fibrillar state. Insulins bound on the elongation surfaces of IAPP fibrils can sterically block the fibril growth via monomer addition. Since the nucleation of amyloid seeds with fibril-like structures is rare, a small number of insulin proteins with high affinity can efficiently bind and cap emerging amyloid seeds during the lag phase and subsequently inhibit the aggregation and delay the lag phase. Together, our results indicated that substoichiometric inhibition could be achieved by targeting the amyloid seeds or protofibrils by capping on the elongation and lateral surfaces and prohibiting the elongation and secondary nucleation. The principle was supported by emerging experimental results, e.g., by analyzing the kinetics of amyloid aggregation, and the clusterin chaperones were found to substoichiometrically retard the aggregation of  $A\beta$  by preferentially binding with the fibril ends and inhibiting the elongation process.44 DNAJB6, a chaperone protein of Hsp40 family, was identified as a substoichiometric inhibitor of the A $\beta$ peptides due to its interactions with the aggregated forms instead of the monomeric form of  $A\beta$ .<sup>45</sup>

The in-register  $\beta$ -sheet structures of IAPP fibrils were found to facilitate insulin binding compared to the disordered IAPP monomers because of the reduction of entropy loss required for binding. This contributed to the extraordinary inhibition

performance of insulin with folded structures compared to other unstructured peptides that failed to exhibit substoichiometric inhibition effects, such as rIAPP and pramlintide.<sup>30</sup> The results suggested that it is possible to enhance the substoichiometric inhibition effect by reducing the entropy cost associated with the conformational conversion of peptidebased inhibitors. Macrocyclic peptides, which reduced the entropy loss to adopt extended  $\beta$ -strand conformation by connecting the N- and C-termini of the designed peptides into cyclic forms, were found to be about 10 times more potent in retarding the lag time of  $A\beta$  aggregation than the free peptides.<sup>46</sup> The enhanced binding affinities between IAPP fibrils and insulins by reducing the entropy loss associated with conformational conversion provided a promising strategy for strengthening the inhibition effect of peptidomimetics by choosing folded proteins or constraining the peptides into aggregation-prone conformations.

#### METHODS

Discrete Molecular Dynamics (DMD) Simulations. Interactions of IAPP and proIAPP with insulin were simulated by all-atom DMD. DMD is a rapid and predictive molecular dynamics algorithm that replaces the continuous interaction potentials in traditional molecular dynamics with optimized discrete stepwise functions. A comprehensive description of the atomistic DMD algorithm can be found in previous publications. <sup>37,38</sup> Briefly, atoms in DMD move with constant velocities until the potential between two atoms is not continuous, where the motions of atoms are instantaneously updated by solving the ballistic equations considering the conservations of energy, momentum, and angular momentum. By implementing a quick sort algorithm to find the collision atoms and only updating the velocities of colliding atoms, DMD can achieve a rapid computational speed and enhanced sampling efficiency. Thus, DMD simulations have been utilized by our group and others to study protein folding, amyloid aggregation, and interactions of proteins/peptides with nanoparticles. The DMD program is available via Molecules in Action, LLC (http://www.moleculesinaction.com/).

Similar to traditional molecular dynamics, bonded interactions (i.e., covalent bonds, bond angles, and dihedrals) and nonbonded interactions (i.e., van der Waals, solvation, hydrogen bond, and electrostatic terms) are considered in our all-atom DMD simulations. The interatomic interactions were adapted from the Medusa force field. The force field parameters for van der Waals, covalent bonds, bond angles, and dihedrals were taken from the CHARMM 19 force field. To reduce the computational cost, implicit solvent model is adopted where the solvation energy is implicitly calculated by the effective energy function proposed by Lazaridis and Karplus. The distance- and angle-dependent hydrogen bond formation is explicitly modeled by a reaction-like algorithm. The screened electrostatic interactions between charged atoms are approximated by the Debye—Hückel model with the Debye length assigned to ~10 Å, which corresponds to a physiological monovalent electrolyte concentration of 100 mM and a water dielectric constant of 80.

The interactions of insulins with (pro)IAPP peptides in monomer, dimer, and fibril states were simulated. The initial structures of proIAPP and IAPP monomers were obtained from the RCSB Protein Data Bank (PDB codes 6UCK and 2L86, respectively, amino acid sequences were shown in Figure 1A) and equilibrated at 300 K for 50  $\mu$ s. The equilibrated monomeric peptides were further incubated with insulins (PDB code 1TRZ) at molar ratios (pro)IAPP/insulin of 1:1 and 1:2. For the interactions between insulin and IAPP fibril, an insulin peptide with folded structure and a 16-peptide fibril based on the S-shaped fibril structure solved by cryo-EM were adopted (PDB code 6ZRF), leading to a substoichiometric concentration IAPP/insulin = 16:1.  $^{41-43}$  The IAPP fibril was fixed to reduce the computational cost, while the insulin peptides can move freely. The folded structure of insulin was preserved by implementing Gō constraints on C $\alpha$  atoms with the native contacts determined if the

 $C\alpha$  atom was within 0.8 nm. The peptides were simulated in a cubic box with the concentration of IAPP peptides fixed at 2.7 mM. Periodic conditions were applied in three directions. Fifty independent simulations starting from random positions and velocities were conducted to enhance the sampling efficiency. Each simulation ran for 1.0  $\mu$ s, accumulating 50.0  $\mu$ s of simulation time for each system.

**Computational Analysis.** The secondary structures of proteins were determined by the DSSP algorithm. Two residues were considered to contact each other if their minimum atomic distance was less than 0.65 nm. The two-dimensional potential of mean force (PMF) was calculated by the probability distribution function, i.e.,  $-k_{\rm B}T\log P(R_{\rm g}n_{\beta{\rm -sheet}})$ , where  $P(R_{\rm g}n_{\beta{\rm -sheet}})$  was the probability of conformations with radius of gyration  $R_{\rm g}$  and number of  $\beta{\rm -sheet}$ residues  $n_{\beta\text{-sheet}}$ . The representative conformations of simulation trajectories were obtained by grouping similar protein conformations using the hierarchical clustering oc program (www.compbio.dundee. ac.uk/downloads/oc). Briefly, the hierarchical clustering algorithm iteratively joined the two closest clusters into one cluster according to the distances between two clusters, which was defined as the mean value of all the pairwise distances between the elements of the two corresponding clusters. The clusters are ranked by their population from high to low, with each cluster represented by its centroid structure, which was selected as the one with the smallest average distance to other elements in the cluster.

#### ASSOCIATED CONTENT

#### Supporting Information

The Supporting Information is available free of charge at https://pubs.acs.org/doi/10.1021/acschemneuro.2c00231.

Secondary structure propensity of each residue for IAPP monomer in the absence and presence of insulin (Figure S1); secondary structure propensity of each proIAPP monomer residue in the absence and presence of insulin (Figure S2); secondary structure propensity of each residue for IAPP and proIAPP dimers (Figure S3); number of residue contacts between insulin and IAPP monomer and IAPP fibril (Figure S4); and kinetics of insulin bound on a IAPP fibril (Figure S5) (PDF)

#### AUTHOR INFORMATION

#### **Corresponding Authors**

Huayuan Tang — Department of Physics and Astronomy, Clemson University, Clemson, South Carolina 29634, United States; Email: huayunt@clemson.edu

Feng Ding — Department of Physics and Astronomy, Clemson University, Clemson, South Carolina 29634, United States; orcid.org/0000-0003-1850-6336; Email: fding@clemson.edu

#### **Author**

Nadav Benhamou Goldfajn — Department of Physics and Astronomy, Clemson University, Clemson, South Carolina 29634, United States; University of Massachusetts, Amherst, Massachusetts 01003, United States; orcid.org/0000-0002-2467-3440

Complete contact information is available at: https://pubs.acs.org/10.1021/acschemneuro.2c00231

#### **Author Contributions**

§N.B.G. and H.T. contributed equally. F.D. conceived the project. N.B.G., H.T., and F.D. performed DMD computer simulations and analysis. N.B.G., H.T., and F.D. wrote the manuscript. All authors agreed on the presentation of the manuscript.

#### **Notes**

The authors declare no competing financial interest.

#### ACKNOWLEDGMENTS

This work was supported by Grant NSF CAREER CBET-1553945 (F.D.) and Grant NIH MIRA R35GM119691 (F.D.). This work was conducted under Clemson University's Biophysics Research Experience for Undergraduates (Grant NSF 1757658). We thank Dr. Joshua Alper and Dr. Hugo Sanabria for directing and organizing the program, and Dr. Ding's lab group members for useful discussions. We thank Professor Pu Chun Ke at Monash University for critical reading of the manuscript.

#### REFERENCES

- (1) Ke, P. C.; Zhou, R.; Serpell, L. C.; Riek, R.; Knowles, T. P. J.; Lashuel, H. A.; Gazit, E.; Hamley, I. W.; Davis, T. P.; Fändrich, M.; Otzen, D. E.; Chapman, M. R.; Dobson, C. M.; Eisenberg, D. S.; Mezzenga, R. Half a Century of Amyloids: Past, Present and Future. *Chem. Soc. Rev.* **2020**, *49*, 5473–5509.
- (2) Milardi, D.; Gazit, E.; Radford, S. E.; Xu, Y.; Gallardo, R. U.; Caflisch, A.; Westermark, G. T.; Westermark, P.; Rosa, C. L.; Ramamoorthy, A. Proteostasis of Islet Amyloid Polypeptide: A Molecular Perspective of Risk Factors and Protective Strategies for Type II Diabetes. *Chem. Rev.* **2021**, *121*, 1845–1893.
- (3) Hieronymus, L.; Griffin, S. Role of Amylin in Type 1 and Type 2 Diabetes. *Diabetes Educ* **2015**, 41, 475–56S.
- (4) Westermark, P.; Andersson, A.; Westermark, G. T. Islet Amyloid Polypeptide, Islet Amyloid, and Diabetes Mellitus. *Physiol. Rev.* **2011**, 91, 795–826.
- (5) Park, K.; Verchere, C. B. Identification of a Heparin Binding Domain in the N-Terminal Cleavage Site of Pro-Islet Amyloid Polypeptide. *J. Biol. Chem.* **2001**, 276, 16611–16616.
- (6) Paulsson, J. F.; Andersson, A.; Westermark, P.; Westermark, G. T. Intracellular Amyloid-like Deposits Contain Unprocessed pro-Islet Amyloid Polypeptide (ProIAPP) in Beta Cells of Transgenic Mice Overexpressing the Gene for Human IAPP and Transplanted Human Islets. *Diabetologia* **2006**, *49*, 1237–1246.
- (7) Meng, F.; Abedini, A.; Song, B.; Raleigh, D. P. Amyloid Formation by Pro-Islet Amyloid Polypeptide Processing Intermediates: Examination of the Role of Protein Heparan Sulfate Interactions and Implications for Islet Amyloid Formation in Type 2 Diabetes. *Biochemistry* **2007**, *46*, 12091–12099.
- (8) Yan, L.-M.; Tatarek-Nossol, M.; Velkova, A.; Kazantzis, A.; Kapurniotu, A. Design of a Mimic of Nonamyloidogenic and Bioactive Human Islet Amyloid Polypeptide (IAPP) as Nanomolar Affinity Inhibitor of IAPP Cytotoxic Fibrillogenesis. *Proc. Natl. Acad. Sci. U.S.A.* **2006**, *103*, 2046–2051.
- (9) Abedini, A.; Meng, F.; Raleigh, D. P. A Single-Point Mutation Converts the Highly Amyloidogenic Human Islet Amyloid Polypeptide into a Potent Fibrillization Inhibitor. *J. Am. Chem. Soc.* **2007**, *129*, 11300–11301.
- (10) Meng, F.; Abedini, A.; Plesner, A.; Verchere, C. B.; Raleigh, D. P. The Flavanol (–)-Epigallocatechin 3-Gallate Inhibits Amyloid Formation by Islet Amyloid Polypeptide, Disaggregates Amyloid Fibrils, and Protects Cultured Cells against IAPP-Induced Toxicity. *Biochemistry* **2010**, *49*, 8127–8133.
- (11) Sciacca, M. F. M.; Chillemi, R.; Sciuto, S.; Greco, V.; Messineo, C.; Kotler, S. A.; Lee, D.-K.; Brender, J. R.; Ramamoorthy, A.; La Rosa, C.; Milardi, D. A Blend of Two Resveratrol Derivatives Abolishes HIAPP Amyloid Growth and Membrane Damage. *Biochimica et Biophysica Acta (BBA) Biomembranes* **2018**, 1860, 1793–1802.
- (12) Kaffy, J.; Berardet, C.; Mathieu, L.; Legrand, B.; Taverna, M.; Halgand, F.; Van Der Rest, G.; Maillard, L. T.; Ongeri, S. Helical  $\gamma$ -Peptide Foldamers as Dual Inhibitors of Amyloid- $\beta$  Peptide and Islet

- Amyloid Polypeptide Oligomerization and Fibrillization. *Chem.—Eur. J.* **2020**, *26*, 14612–14622.
- (13) Thorn, D. C.; Meehan, S.; Sunde, M.; Rekas, A.; Gras, S. L.; MacPhee, C. E.; Dobson, C. M.; Wilson, M. R.; Carver, J. A. Amyloid Fibril Formation by Bovine Milk  $\kappa$ -Casein and Its Inhibition by the Molecular Chaperones  $\alpha$  <sub>S</sub> and  $\beta$ -Casein. *Biochemistry* **2005**, *44*, 17027–17036.
- (14) McLaurin, J.; Cecal, R.; Kierstead, M. E.; Tian, X.; Phinney, A. L.; Manea, M.; French, J. E.; Lambermon, M. H. L.; Darabie, A. A.; Brown, M. E.; Janus, C.; Chishti, M. A.; Horne, P.; Westaway, D.; Fraser, P. E.; Mount, H. T. J.; Przybylski, M.; St George-Hyslop, P. Therapeutically Effective Antibodies against Amyloid- $\beta$  Peptide Target Amyloid- $\beta$  Residues 4–10 and Inhibit Cytotoxicity and Fibrillogenesis. *Nat. Med.* **2002**, *8*, 1263–1269.
- (15) Ladiwala, A. R. A.; Bhattacharya, M.; Perchiacca, J. M.; Cao, P.; Raleigh, D. P.; Abedini, A.; Schmidt, A. M.; Varkey, J.; Langen, R.; Tessier, P. M. Rational Design of Potent Domain Antibody Inhibitors of Amyloid Fibril Assembly. *Proc. Natl. Acad. Sci. U. S. A.* **2012**, *109*, 19965–19970.
- (16) Gladytz, A.; Abel, B.; Risselada, H. J. Gold-Induced Fibril Growth: The Mechanism of Surface-Facilitated Amyloid Aggregation. *Angew. Chem., Int. Ed.* **2016**, *55*, 11242–11246.
- (17) Gurzov, E. N.; Wang, B.; Pilkington, E. H.; Chen, P.; Kakinen, A.; Stanley, W. J.; Litwak, S. A.; Hanssen, E. G.; Davis, T. P.; Ding, F.; Ke, P. C. Inhibition of HIAPP Amyloid Aggregation and Pancreatic  $\beta$ -Cell Toxicity by OH-Terminated PAMAM Dendrimer. *Small* **2016**, 12, 1615–1626.
- (18) Javed, I.; Sun, Y.; Adamcik, J.; Wang, B.; Kakinen, A.; Pilkington, E. H.; Ding, F.; Mezzenga, R.; Davis, T. P.; Ke, P. C. Cofibrillization of Pathogenic and Functional Amyloid Proteins with Gold Nanoparticles against Amyloidogenesis. *Biomacromolecules* 2017, 18, 4316–4322.
- (19) Koppel, K.; Tang, H.; Javed, I.; Parsa, M.; Mortimer, M.; Davis, T. P.; Lin, S.; Chaffee, A. L.; Ding, F.; Ke, P. C. Elevated Amyloidoses of Human IAPP and Amyloid Beta by Lipopolysaccharide and Their Mitigation by Carbon Quantum Dots. *Nanoscale* **2020**, *12*, 12317–12328.
- (20) Li, Y.; Tang, H.; Zhu, H.; Kakinen, A.; Wang, D.; Andrikopoulos, N.; Sun, Y.; Nandakumar, A.; Kwak, E.; Davis, T. P.; Leong, D. T.; Ding, F.; Ke, P. C. Ultrasmall Molybdenum Disulfide Quantum Dots Cage Alzheimer's Amyloid Beta to Restore Membrane Fluidity. ACS Appl. Mater. Interfaces 2021, 13, 29936—29948
- (21) Scrocchi, L. A.; Chen, Y.; Waschuk, S.; Wang, F.; Cheung, S.; Darabie, A. A.; McLaurin, J.; Fraser, P. E. Design of Peptide-Based Inhibitors of Human Islet Amyloid Polypeptide Fibrillogenesis. *J. Mol. Biol.* **2002**, *318*, 697–706.
- (22) Goyal, D.; Shuaib, S.; Mann, S.; Goyal, B. Rationally Designed Peptides and Peptidomimetics as Inhibitors of Amyloid- $\beta$  ( $A\beta$ ) Aggregation: Potential Therapeutics of Alzheimer's Disease. *ACS Comb. Sci.* **2017**, *19*, 55–80.
- (23) Laxio Arenas, J.; Kaffy, J.; Ongeri, S. Peptides and Peptidomimetics as Inhibitors of Protein-Protein Interactions Involving  $\beta$ -Sheet Secondary Structures. *Curr. Opin Chem. Biol.* **2019**, 52, 157–167.
- (24) Richman, M.; Wilk, S.; Chemerovski, M.; Wärmländer, S. K. T. S.; Wahlström, A.; Gräslund, A.; Rahimipour, S. In Vitro and Mechanistic Studies of an Antiamyloidogenic Self-Assembled Cyclic D, L -α-Peptide Architecture. *J. Am. Chem. Soc.* **2013**, *135*, 3474–3484.
- (25) Spanopoulou, A.; Heidrich, L.; Chen, H.-R.; Frost, C.; Hrle, D.; Malideli, E.; Hille, K.; Grammatikopoulos, A.; Bernhagen, J.; Zacharias, M.; Rammes, G.; Kapurniotu, A. Designed Macrocyclic Peptides as Nanomolar Amyloid Inhibitors Based on Minimal Recognition Elements. *Angew. Chem., Int. Ed.* **2018**, *57*, 14503–14508.
- (26) Scollo, F.; Tempra, C.; Lolicato, F.; Sciacca, M. F. M.; Raudino, A.; Milardi, D.; La Rosa, C. Phospholipids Critical Micellar Concentrations Trigger Different Mechanisms of Intrinsically

- Disordered Proteins Interaction with Model Membranes. J. Phys. Chem. Lett. 2018, 9, 5125-5129.
- (27) Sciacca, M. F.; Lolicato, F.; Tempra, C.; Scollo, F.; Sahoo, B. R.; Watson, M. D.; García-Viñuales, S.; Milardi, D.; Raudino, A.; Lee, J. C.; Ramamoorthy, A.; La Rosa, C. Lipid-Chaperone Hypothesis: A Common Molecular Mechanism of Membrane Disruption by Intrinsically Disordered Proteins. ACS Chem. Neurosci. 2020, 11, 4336–4350.
- (28) Cao, P.; Abedini, A.; Wang, H.; Tu, L.-H.; Zhang, X.; Schmidt, A. M.; Raleigh, D. P. Islet Amyloid Polypeptide Toxicity and Membrane Interactions. *Proc. Natl. Acad. Sci. U.S.A.* **2013**, *110*, 19279–19284.
- (29) Tomasello, M. F.; Sinopoli, A.; Attanasio, F.; Giuffrida, M. L.; Campagna, T.; Milardi, D.; Pappalardo, G. Molecular and Cytotoxic Properties of HIAPP17–29 and RIAPP17–29 Fragments: A Comparative Study with the Respective Full-Length Parent Polypeptides. *Eur. J. Med. Chem.* **2014**, *81*, 442–455.
- (30) Wang, H.; Ridgway, Z.; Cao, P.; Ruzsicska, B.; Raleigh, D. P. Analysis of the Ability of Pramlintide To Inhibit Amyloid Formation by Human Islet Amyloid Polypeptide Reveals a Balance between Optimal Recognition and Reduced Amyloidogenicity. *Biochemistry* 2015, 54, 6704–6711.
- (31) Larson, J. L.; Miranker, A. D. The Mechanism of Insulin Action on Islet Amyloid Polypeptide Fiber Formation. *J. Mol. Biol.* **2004**, *335*, 221–231.
- (32) Wang, H.; Raleigh, D. P. The Ability of Insulin to Inhibit the Formation of Amyloid by Pro-Islet Amyloid Polypeptide Processing Intermediates Is Significantly Reduced in the Presence of Sulfated Glycosaminoglycans. *Biochemistry* **2014**, *53*, 2605–2614.
- (33) Gilead, S.; Wolfenson, H.; Gazit, E. Molecular Mapping of the Recognition Interface between the Islet Amyloid Polypeptide and Insulin. *Angew. Chem.* **2006**, *118*, 6626–6630.
- (34) Baram, M.; Gilead, S.; Gazit, E.; Miller, Y. Mechanistic Perspective and Functional Activity of Insulin in Amylin Aggregation. *Chem. Sci.* **2018**, *9*, 4244–4252.
- (35) Nedumpully-Govindan, P.; Ding, F. Inhibition of IAPP Aggregation by Insulin Depends on the Insulin Oligomeric State Regulated by Zinc Ion Concentration. *Sci. Rep* **2015**, *5*, 8240.
- (36) Krampert, M.; Bernhagen, J.; Schmucker, J.; Horn, A.; Schmauder, A.; Brunner, H.; Voelter, W.; Kapurniotu, A. Amyloidogenicity of Recombinant Human Pro-Islet Amyloid Polypeptide (ProIAPP). Chem. Biol. 2000, 7, 855–871.
- (37) Ding, F.; Tsao, D.; Nie, H.; Dokholyan, N. V. Ab Initio Folding of Proteins with All-Atom Discrete Molecular Dynamics. *Structure* **2008**, *16*, 1010–1018.
- (38) Ding, F.; Dokholyan, N. V. Discrete Molecular Dynamics Simulation of Biomolecules. In *Computational Modeling of Biological Systems*; Dokholyan, N. V., Ed.; Biological and Medical Physics, Biomedical Engineering; Springer US: Boston, MA, 2012; pp 55–73, DOI: 10.1007/978-1-4614-2146-7 3.
- (39) Jaikaran, E. T. A. S.; Higham, C. E.; Serpell, L. C.; Zurdo, J.; Gross, M.; Clark, A.; Fraser, P. E. Identification of a Novel Human Islet Amyloid Polypeptide  $\beta$ -Sheet Domain and Factors Influencing Fibrillogenesis. *J. Mol. Biol.* **2001**, *308*, 515–525.
- (40) Buchanan, L. E.; Dunkelberger, E. B.; Tran, H. Q.; Cheng, P.-N.; Chiu, C.-C.; Cao, P.; Raleigh, D. P.; de Pablo, J. J.; Nowick, J. S.; Zanni, M. T. Mechanism of IAPP Amyloid Fibril Formation Involves an Intermediate with a Transient -Sheet. *Proc. Natl. Acad. Sci. U. S. A.* **2013**, *110*, 19285–19290.
- (41) Röder, C.; Kupreichyk, T.; Gremer, L.; Schäfer, L. U.; Pothula, K. R.; Ravelli, R. B. G.; Willbold, D.; Hoyer, W.; Schröder, G. F. Cryo-EM Structure of Islet Amyloid Polypeptide Fibrils Reveals Similarities with Amyloid- $\beta$  Fibrils. *Nat. Struct Mol. Biol.* **2020**, *27*, 660–667.
- (42) Gallardo, R.; Iadanza, M. G.; Xu, Y.; Heath, G. R.; Foster, R.; Radford, S. E.; Ranson, N. A. Fibril Structures of Diabetes-Related Amylin Variants Reveal a Basis for Surface-Templated Assembly. *Nat. Struct Mol. Biol.* **2020**, *27*, 1048–1056.
- (43) Cao, Q.; Boyer, D. R.; Sawaya, M. R.; Abskharon, R.; Saelices, L.; Nguyen, B. A.; Lu, J.; Murray, K. A.; Kandeel, F.; Eisenberg, D. S.

Cryo-EM Structures of HIAPP Fibrils Seeded by Patient-Extracted Fibrils Reveal New Polymorphs and Conserved Fibril Cores. *Nat. Struct Mol. Biol.* **2021**, 28, 724–730.

- (44) Scheidt, T.; Łapińska, U.; Kumita, J. R.; Whiten, D. R.; Klenerman, D.; Wilson, M. R.; Cohen, S. I. A.; Linse, S.; Vendruscolo, M.; Dobson, C. M.; Knowles, T. P. J.; Arosio, P. Secondary Nucleation and Elongation Occur at Different Sites on Alzheimer's Amyloid-β Aggregates. Sci. Adv. 2019, 5, eaau3112.
- (45) Månsson, C.; Arosio, P.; Hussein, R.; Kampinga, H. H.; Hashem, R. M.; Boelens, W. C.; Dobson, C. M.; Knowles, T. P. J.; Linse, S.; Emanuelsson, C. Interaction of the Molecular Chaperone DNAJB6 with Growing Amyloid-Beta 42 ( $A\beta$ 42) Aggregates Leads to Sub-Stoichiometric Inhibition of Amyloid Formation. *J. Biol. Chem.* **2014**, 289, 31066–31076.
- (46) Lu, J.; Cao, Q.; Wang, C.; Zheng, J.; Luo, F.; Xie, J.; Li, Y.; Ma, X.; He, L.; Eisenberg, D.; Nowick, J.; Jiang, L.; Li, D. Structure-Based Peptide Inhibitor Design of Amyloid- $\beta$  Aggregation. *Front. Mol. Neurosci.* **2019**, *12*, 54.
- (47) Brooks, B. R.; Bruccoleri, R. E.; Olafson, B. D.; States, D. J.; Swaminathan, S.; Karplus, M. CHARMM: A Program for Macromolecular Energy, Minimization, and Dynamics Calculations. *J. Comput. Chem.* **1983**, *4*, 187–217.
- (48) Lazaridis, T. Effective Energy Functions for Protein Structure Prediction. *Curr. Opin. Struct. Biol.* **2000**, *10*, 139–145.
- (49) Ding, F.; Borreguero, J. M.; Buldyrey, S. V.; Stanley, H. E.; Dokholyan, N. V. Mechanism for the ?-Helix to ?-Hairpin Transition. *Proteins* **2003**, *53*, 220–228.
- (50) DeLisle, C. F.; Malooley, A. L.; Banerjee, I.; Lorieau, J. L. Pro-Islet Amyloid Polypeptide in Micelles Contains a Helical Prohormone Segment. *FEBS Journal* **2020**, 287, 4440–4457.
- (51) Kabsch, W.; Sander, C. Dictionary of Protein Secondary Structure: Pattern Recognition of Hydrogen-Bonded and Geometrical Features. *Biopolymers* **1983**, *22*, 2577–2637.

### ☐ Recommended by ACS

### Disparate Effect of Hybrid Peptidomimetics Containing Isomers of Aminobenzoic Acid on hIAPP Aggregation

Rituparna Roy and Sandip Paul

DECEMBER 02, 2022

THE JOURNAL OF PHYSICAL CHEMISTRY B

READ 🗹

### Differential Effects of Aromatic Residues on Amyloid Formation and Cytotoxicity of Human IAPP

Lakshan Manathunga, Daniel P. Raleigh, et al.

OCTOBER 10, 2022

BIOCHEMISTRY

READ 🗹

### Molecular Dynamics Simulations Indicate Aromaticity as a Key Factor in the Inhibition of $IAPP_{(20-29)}$ Aggregation

Kelsie M. King, Anne M. Brown, et al.

MAY 19, 2022

ACS CHEMICAL NEUROSCIENCE

READ 🗹

## Multiple Actions of H<sub>2</sub>S-Releasing Peptides in Human β-Amyloid Expressing *C. elegans*

Rafat Ali, Sandeep Verma, et al.

NOVEMBER 09, 2022

ACS CHEMICAL NEUROSCIENCE

READ **C** 

Get More Suggestions >